Technical Report ARAED-TR-92021

ENERGY DEPOSITION FROM A SHAPED CHARGE JET

Barry Fishburn

October 1992

US ARMY ARMAMENT MUNITIONS & CHEMICAL COMMAND ARMAMENT RDE CENTER

U.S. ARMY ARMAMENT RESEARCH, DEVELOPMENT AND ENGINEERING CENTER

Armament Engineering Directorate

Picatinny Arsenal, New Jersey

The views, opinions, and/or findings contained in this report are those of the authors(s) and should not be construed as an official Department of the Army position, policy, or decision, unless so designated by other documentation.

The citation in this report of the names of commercial firms or commercially available products or services does not constitute official endorsement by or approval of the U.S. Government.

Destroy this report when no longer needed by any method that will prevent disclosure of its contents or reconstruction of the document. Do not return to the originator.

THIS
PAGE
IS
MISSING
IN
ORIGINAL
DOCUMENT

REPORT DOCUMENTATION PAGE	Form Approved OMB No. 0704-0188

1. AGENCY USE ONLY (Leave blank)	2. REPORT DATE	3. REPORT TYPE AND DATES COVERED
	October 1992	

4. TITLE AND SUBTITLE
ENERGY DEPOSITION FROM A SHAPED CHARGE JET

5. FUNDING NUMBERS

6. AUTHOR(S)
Barry Fishburn

7. PERFORMING ORGANIZATION NAME(S) AND ADDRESSES(S)
ARDEC, AED
Energetics and Warhead Division (SMCAR-AEE-WW)
Picatinny Arsenal, NJ 07806-5000

8. PERFORMING ORGANIZATION REPORT NUMBER
Technical Report
ARAED-TR-92021

9 SPONSORING/MONITORING AGENCY NAME(S) AND ADDRESS(S)
ARDEC, IMD
STINFO Br (SMCAR-IMI-I)
Picatinny Arsenal, NJ 07806-5000

10. SPONSORING/MONITORING AGENCY REPORT NUMBER

11. SUPPLEMENTARY NOTES

12a DISTRIBUTION/AVAILABILITY STATEMENT

Approved for public release; distribution is unlimited.

12b. DISTRIBUTION CODE

13. ABSTRACT (Maximum 200 words)

A fast, easy method of calculating energy deposition during shaped charge jet penetration was developed to assist in jet impact testing of energetic matenals. Particularly, the profile of energy deposition along the penetration path is obtained. The ability to generate these profiles for every test setup allows test personnel to quantitatively analyze their data with a minimum of effort and clearly distinguishes how the stimulus varies when different shaped charges are substituted during testing.

14. SUBJECT TERMS
Jet penetration
Jet energy deposition
Jet impact testing

15. NUMBER OF PAGES
27

16. PRICE CODE

17. SECURITY CLASSIFICATION OF REPORT	18. SECURITY CLASSIFICATION OF THIS PAGE	19. SECURITY CLASSIFICATION OF ABSTRACT	20. LIMITATION OF ABSTRACT
UNCLASSIFIED	UNCLASSIFIED	UNCLASSIFIED	SAR

CONTENTS

FIGURES

FIGURES (Continued)

INTRODUCTION

Shaped charge jets are being used as initiating stimuli in tests of energetic materials. The response of these materials can vary considerably, depending on which shaped charge is used in the test. One jet parameter which seems to be of importance is the energy that the jet deposits in the target. This energy is spread out over the penetration path in a complicated way and a means to calculate this energy profile was needed. Thus the hydrodynamic penetration theory was employed to calculate these energy deposition profiles to assess effects of standoff and various combinations of conditioning plates on the stimulus level seen by test samples.

METHOD

Calculations of energy deposition were carried out using the hydrodynamic penetration model. The energy deposited by the jet in penetrating an infinitesimal distance dp is just the kinetic energy of the jet which is used up in obtaining this dp. Thus, the energy deposition can be shown to be

$$\frac{dE}{dp} = \frac{1}{2}\sqrt{r_j r_t}\, U_j^2 A_j \qquad (1)$$

where U_j and A_j are instantaneous values of jet velocity and cross-sectional area at the stagnation point of the penetration cavity while r_t and r_j are the respective jet and target densities.

The cross-sectional area of the jet constantly changes due to jet stretching. At a fixed Lagrangian point on the jet (which we choose to measure using the accumulated jet mass), the area change is given by

$$\frac{dA_j}{dt} = r_j A_j^2 \frac{dU_j}{dm}$$

where m is the accumulated mass in the jet, measured back from the tip. If we invoke the usual assumption that the velocity of a jet particle does not change during flight, then dU_j/dm is not a function of t and the jet area is given by

$$A_j = \frac{A_0}{1 - r_j A_0 \frac{dU_j}{dm}(t - t_0)} \qquad (2)$$

with integration constants A_0 and t_0. While penetrating a target, the rate at which mass is used up is given by

$$\frac{dm}{dt} = r_j A_j \frac{\mu}{1+\mu} U_j \qquad (3)$$

with $$\mu = \sqrt{\frac{\rho_t}{\rho_j}}.$$

After substitution of equation 2, the expression for mass loss is

$$\frac{dm}{dt} = \frac{\rho_j \frac{\mu}{1+\mu} A_0 U_j}{1 - \rho_j A_0 \frac{dU_j}{dm}(t - t_0)} \tag{4}$$

where U_j, A_0 and dU_j/dm are only functions of m. A simple integral of penetration velocity gives penetration depth,

$$P = \int_{t_1}^{t_2} \frac{U_j}{1+\mu} dt \tag{5}$$

In this formulation, the shaped charge jet is completely described by stipulating velocity and cross-sectional area at a given time as a function of accumulated mass. There are numerous ways to handle the required initial conditions. One possibility is to calculate the cross section when the element of jet forms and record the time when it forms as a function of accumulated mass up to this point. Another approach is to use a jet snapshot to measure area, in which case t_0 is the same for each jet element. This latter method was used here and the time of the snapshot is relative to the instant when the first jet particle forms.

Note that the equation 2 can be used to calculate (dU_j/dm) if two x-ray snapshots of a jet are taken at different times. The time interval is chosen large enough that the jet area change is easy to measure. With area from the earliest snapshot and (dU_j/dm) from equation 2, a complete initial condition data set is established.

VIRTUAL ORIGIN ASSUMPTION

Some simplifications can be obtained if the virtual origin jet assumption is invoked. A virtual origin jet has a linear velocity distribution so that

$$\frac{\partial U_j}{\partial x} = -f(t) \quad \text{or} \quad U_j = -f(t)\,x + U_{tip} \tag{6}$$

At any instant of time, t_0

$$\frac{\partial m}{\partial U_j} = \frac{\partial m}{\partial x}\frac{\partial x}{\partial U_j} = \rho_j A_0 \left(-\frac{1}{f(t_0)}\right)$$

However, accumulated mass is a Lagrangian coordinate so that

$$\frac{\partial m}{\partial U_j} = \frac{dm}{dU_j}$$

and thus

$$A_0 \frac{dU_j}{dm} = -\frac{f(t_0)}{r_j}$$

is a constant. Then equation 4 can be integrated to give the velocity at the bottom of the penetration cavity, viz.

$$\frac{U_j}{U_{tip}} = \left[1 + f(t_0)(t-t_0)\right]^{-\frac{\mu}{\mu+1}}$$

Now equation 5 is integrated using this expression to give

$$P = \frac{U_{tip}}{f(t_0)} \left\{ \left[1 + f(t_0)\, t_0 \left(\frac{t}{t_0} - 1 \right) \right]^{\frac{1}{\mu+1}} \right\}.$$

Choose t_0 as the time when the jet tip hits the target. The time from the virtual origin to the target is found from

$$t_0 = \frac{x_{tip} - x_r}{U_{tip} - U_r}$$

with $(\cdot)_r$ referring to the last element of the jet, which, after substituting for the velocity difference from equation 6 leads to

$$t_0 = \frac{1}{f(t_0)}$$

giving the usual form of the Allison - Vitali formula (ref 1, p.138), viz.

$$P = U_{tip}\, t_0 \left[\left(\frac{t}{t_0} \right)^{\frac{1}{1+\mu}} - 1 \right]$$

Calculations of Energy Deposition Rates for Several Jets

Ernest Baker of ARDEC provided a copy of the analytical shaped charge code PASCC1 (ref 2), which he developed, (and also tutorials to the author which allowed successful use of his code) to calculate jet formation conditions for several charges. Another code was written to integrate equations 4 and 5 using the output from PASCC1. Some results are discussed below.

First, a viper jet was calculated using PASCC1. Insufficient detail of the cone apex was included for PASCC1 to predict any tip particle phenomena for this jet. The calculated effect of standoff on energy dissipation for a Viper shaped charge against a homogeneous target with density of 1.1 gm/cc located at 36.83 cm (14.5 inches) from the base of the Viper is shown in figure 1. A curious feature is that energy deposition peaks at some distance into the target because jet area increases at the stagnation point more rapidly than the square of velocity falls off, according to the calculation. Standoff has almost no effect after about 25 cm of target has been penetrated.

The calculated effect of various thickness of steel conditioning plate is shown in figure 2. These plates are assumed to be located 12.7 cm (five inches) from the charge, while the 1.1 gm/cc target is still located at 36.83 cm. Thin plates wipe off the early portion of the jet causing the large area portion to hit target material at a lesser distance than if the early material were allowed to impact the target. The jet cross section has less time to shrink, which causes the maximum value of energy dissipation to be higher with the thinest plate than without it. It becomes clear that energy deposition is sensitive to details of the jet structure.

A comparison of three typical charges, all at 36.83 cm standoff from the 1.1 gm/cc target is shown in figure 3. Energy deposition by the BRL-81 mm runs about 50% above the Viper. The Tow2a produces a jet with wildly varying radius. The thin early jet cannot deliver much energy to the target, but the rate of energy delivery increases rapidly. There are large particles in the Tow2a jet, caused by reverse velocity gradients created during jet formation, which travel without stretching and deliver large energy input to the target as they impact. The figure shows that two of these particles should impact within the 0.5 meters thickness of the target. Obviously, the Tow2a delivers a completely different energy imput profile as compared to the other two charges and the particles dominate energy deposition.

Since the virtual origin approximation is so widely used, it is worthwhile to calculate the energy deposited by a virtual origin jet having the Viper's velocity gradient and mass. In order to calculate energy deposition for virtual origin jets, a knowlege of how their cross-sectional area varies along the jet is needed. As an

example, pick the simplest possible case, i.e., assume that the jet has constant radius along its length at any instant of time, then its energy deposition is easily calculated, and is given by

$$\frac{dE}{dP} = \frac{1}{2}\sqrt{r_t r_j}\, U_{tip}^{\,2} A_0 \left(\frac{P}{S}+1\right)^{-(3\mu+1)} \qquad (7)$$

$$E = \frac{1}{2} r_j U_{tip}^{\,2} \left(\frac{A_0 S}{3}\right)\left[1-\left(\frac{P}{S}+1\right)^{-3\mu}\right]$$

The value of A_0S is calculated from

$$A_0 S = \frac{1}{r_j}\frac{U_{tip}}{U_{tip}-U_r} m$$

with m the accumulated mass up to the particular element chosen as the rearmost element (note that this product is constant as the jet stretches). The standoff, S, is calculated from the PASCC1 Viper output in the following way. The PASCC1 output gives jet velocity as a function of axial distance as a snapshot picture at some particular time. Let x_1 be the distance of the tip from the cone reference point, the point where the first jet particle is formed. The distance of the tip from its virtual origin can be found from

$$\tilde{S} = \frac{U_{tip}}{U_{tip}-U_r} h$$

where h is the distance from the tip to the chosen rear element which has velocity U_r (taken nominally as 2.5 K/S). Then, if x_2 is the distance from charge base to the target and x_3 is the distance from the charge base to the cone reference point, the target standoff distance is

$$S = x_2 + x_3 + \tilde{S} - x_1$$

Formula 7 is plotted in figure 4 along with the calculated results from PASCC1. The constant area, virtual origin jet deviates from the PASCC1 jet for the first 15 cm of target penetration and this deviation is considerable. Net deposited energy generally varies with the square of tip velocity, but is notably sensitive to the area distribution along the jet.

Experimental Viper Jet

Mr. James Pham of ARDEC provided a double exposed x-ray of a viper jet for analysis. The x-ray shows the jet at 28.904 microseconds and 49.329 microseconds relative to the instant that the first piece of jet forms. Note that the firing pulse occurs at

-12.146 microseconds on this time scale, so the time relative to the firing pulse has this value added on. Both jet images were digitized and the results are shown in figures 5 and 6. A best estimate for the axis of symmetry was made by fitting curves between the points away from the tip. As can be seen, the resulting axis nicely pass through the center of the tip also. Based on these axis, the axisymmetric volume at each time was determined as a function of distance from the tip. The resulting jet radius and jet mass (volume times density) are shown in figures 7 and 8. Consistent with the hydrodynamic development used here, it is assumed that the point described by "m" grams back from the tip of one x-ray is also "m" grams back in the other. Thus, the assumption is that no inversion of mass coordinates occurs during flight. The difference in radii between x-rays is nominally 20%, so that small errors in reading the data are not crucial. Equation 2 can now be used to calculate dU_j/dm as a function of accumulated mass (fig. 9) and ultimately jet velocity (fig. 10). The range of the accumulated mass coordinate is limited by how much of the early jet appears in the x-ray. Results of this procedure give a smooth velocity profile with two small regions of reverse gradient. The x-ray tip velocity is faster than that calculated by PASCC1 as can be seen when comparing velocity distributions in figure 11. The velocity gradient after mass coordinate =.002 kg is similar to, but slightly steeper than that calculated by PASCC1. A comparison of the jet radii from the x-ray with that calculated by PASCC1 is shown in figure 12. The x-ray results appear to agree with the calculation except in the tip region. Energy deposition, calculated using these experimental data, is shown on figure 13. Obviously, the tip delivers a lot of energy. Energy deposition drops to that from PASCC1 after the tip is absorbed. These results on a larger scale are shown in figure 14. It seems the PASCC1 results can be used satisfactorily beyond about 4 cm penetration. The effect of a 1.27 cm steel conditioning plate on the x-ray derived jet data is shown in figure 15. The large tip effect is essentially removed by this conditioning plate.

CONCLUSION

With the use of various shaped charges as initiating stimuli for probing assorted energetic materials, the ability to quantify the strength of stimulus becomes important for comparing results and in forming a basis for understanding what parameters govern the response of the energetic material. This hydrodynamic analysis gives a quick way to quantify the stimulus for any test setup and also serves to point up how sensitive the stimulus parameters can be to details of the jet. It is particularly useful to study cases where stimulated reaction appears only along part of the path of the jet through the target. The point of cessation of reaction can be correlated with local jet properties. Of course, this analysis is only as good as the basic jet description and developing an accurate jet description should be pursued.

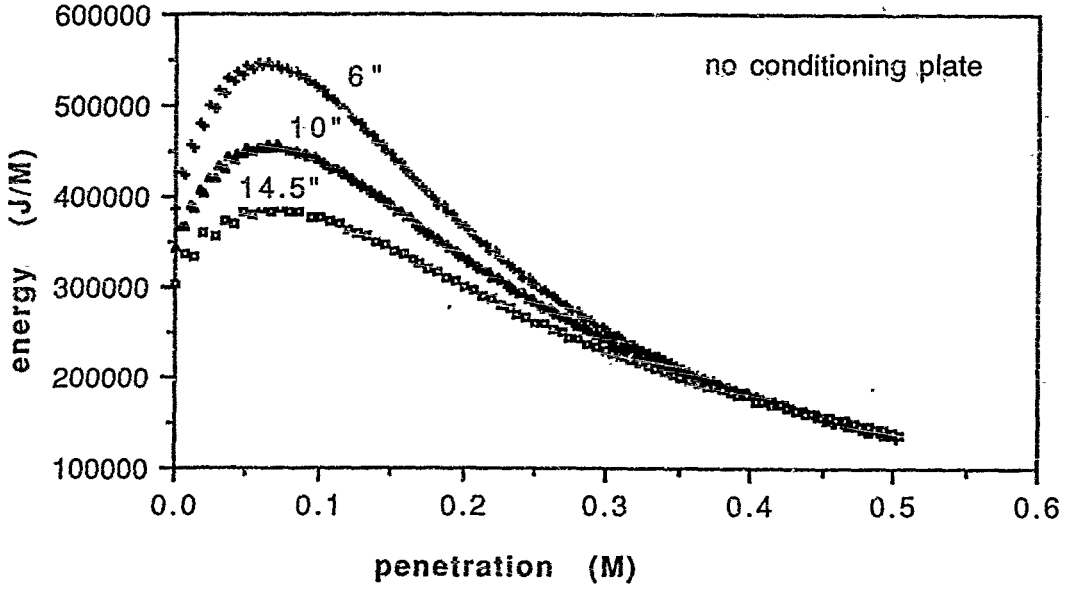

Figure 1. Effect of standoff on Viper

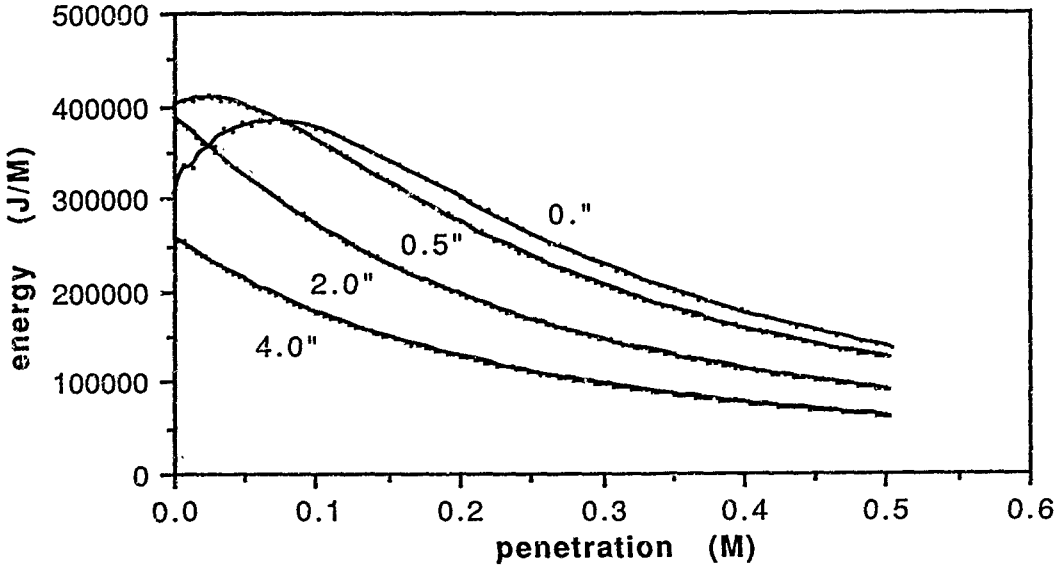

Figure 2. Effect of conditioning plates

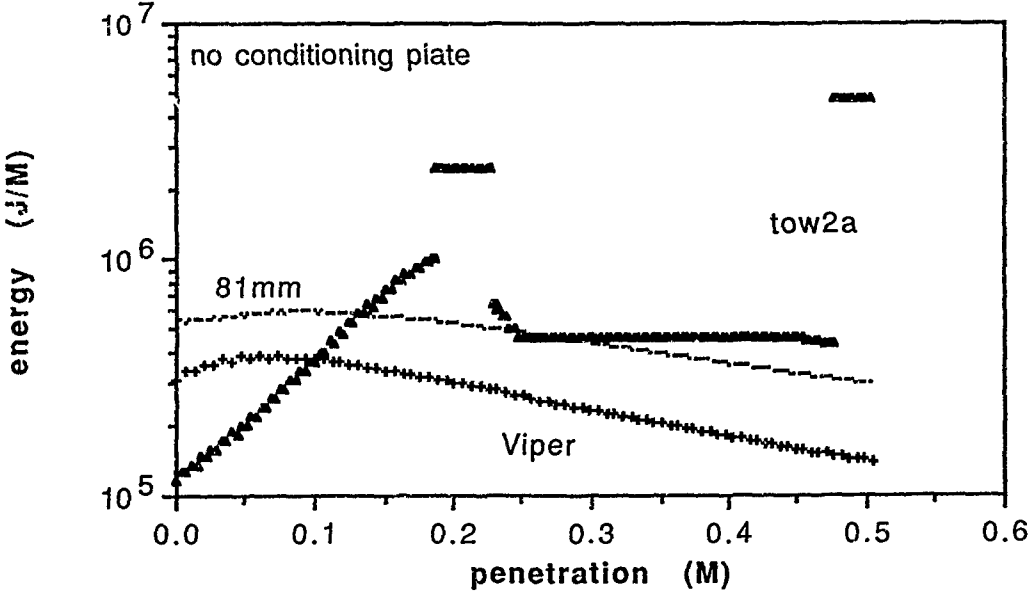

Figure 3. Three jets

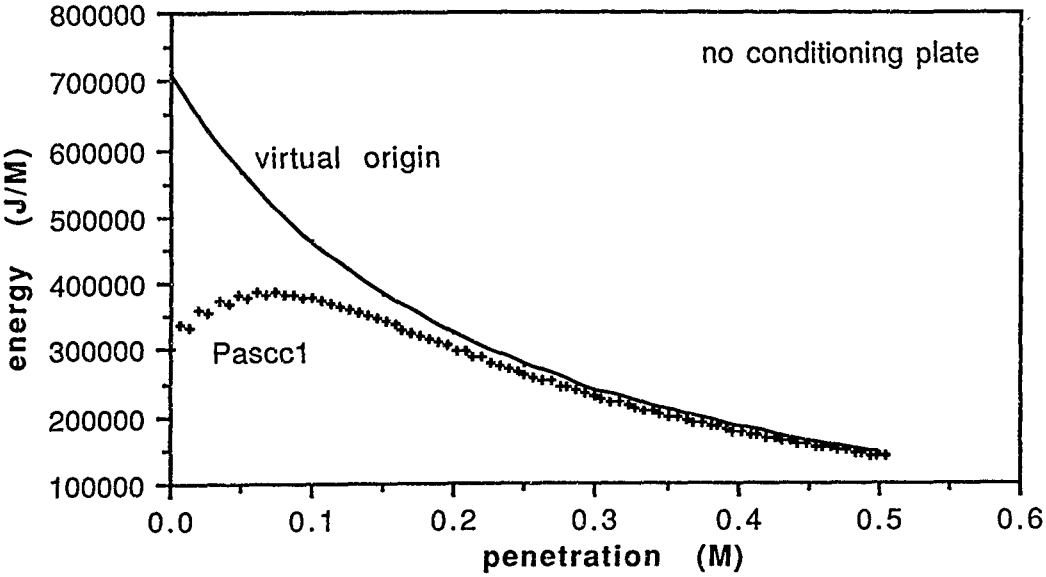

Figure 4. Viper comparisons

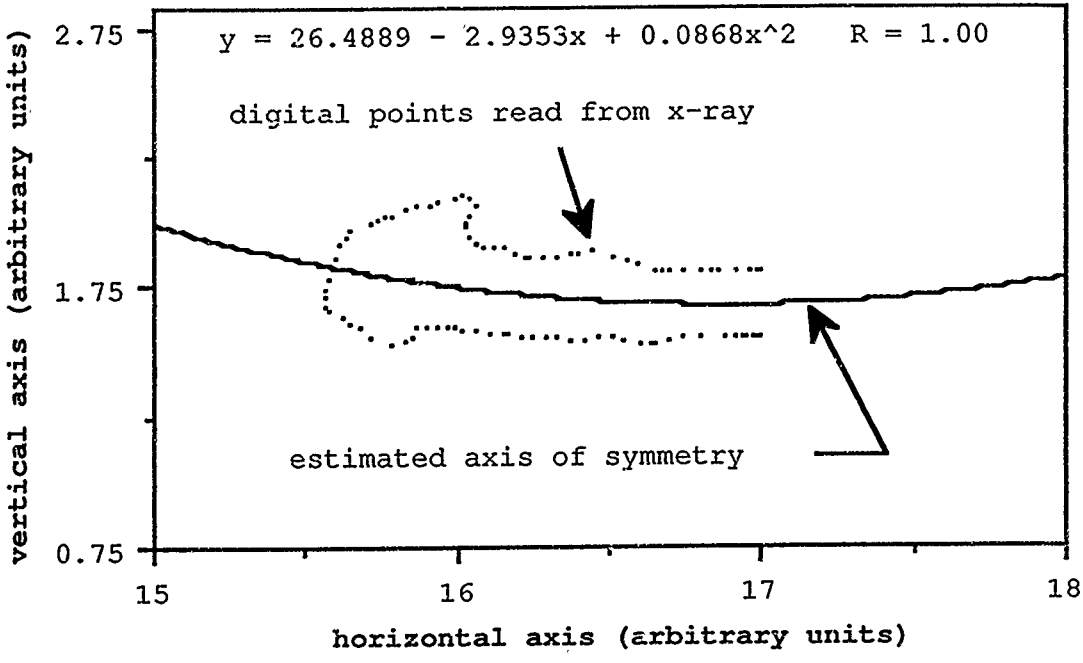

Figure 5. Jet at 41.05 microseconds

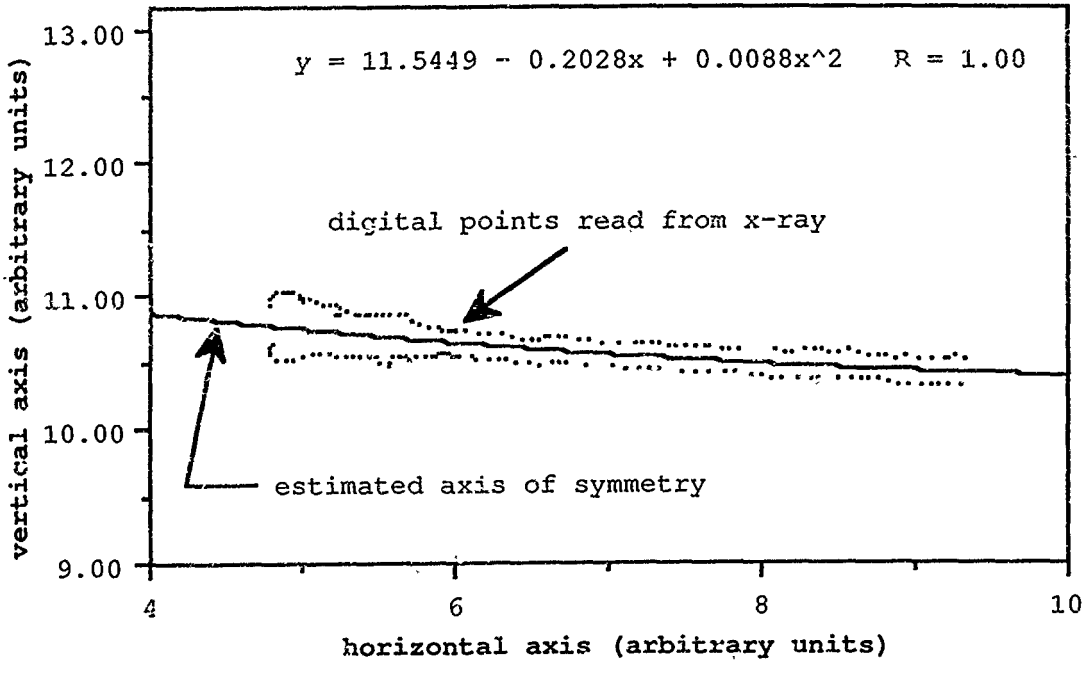

Figure 6. Jet at 61.475 microseconds

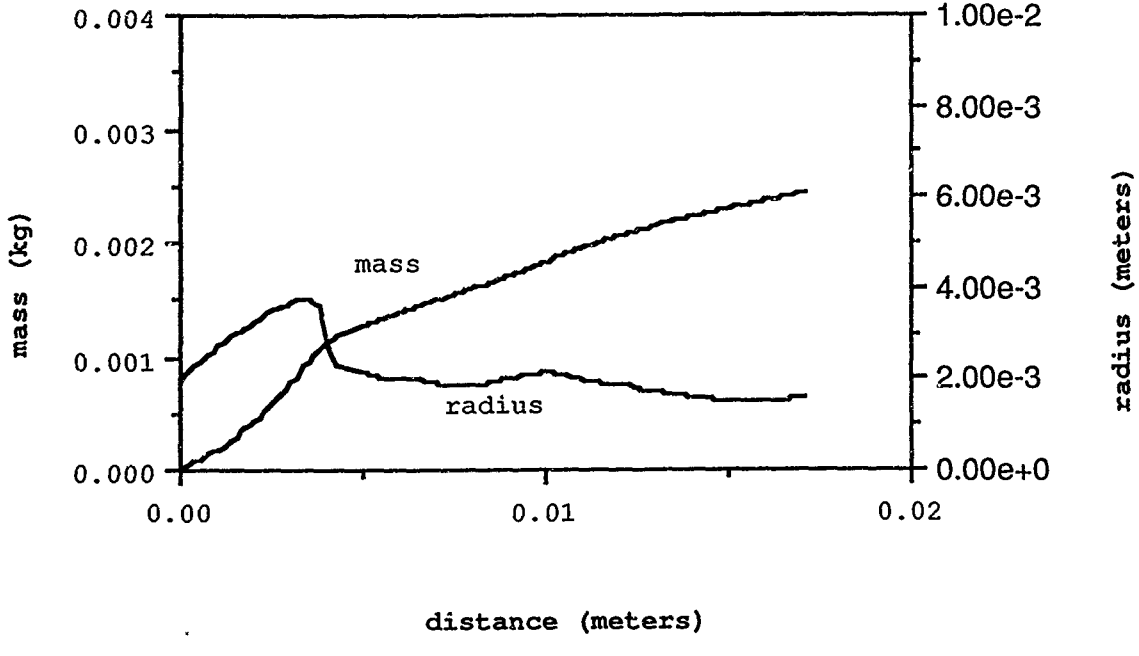

Figure 7. Analysis of jet at 41.05 microseconds

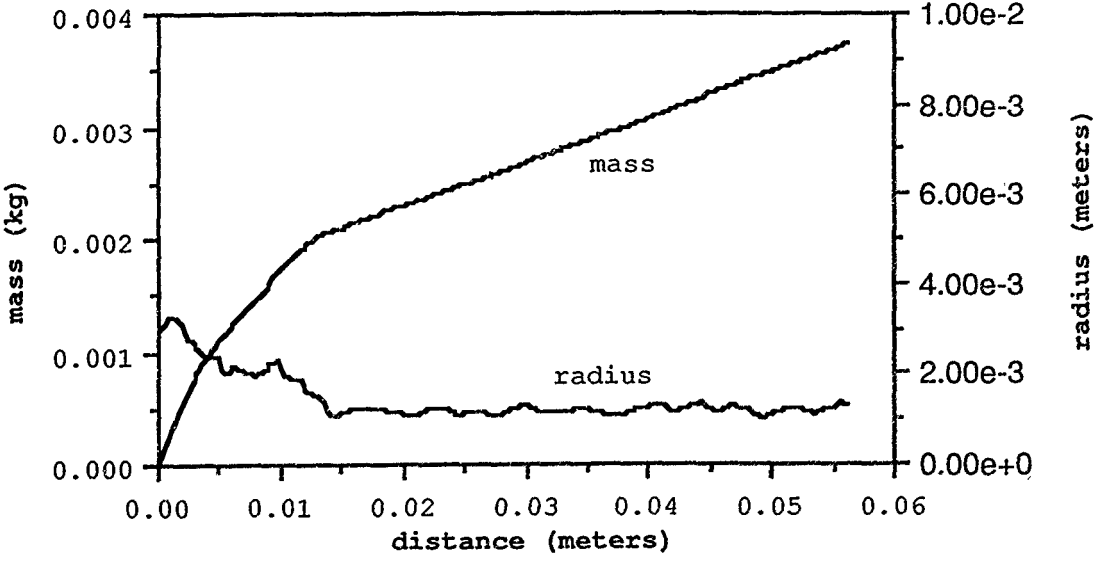

Figure 8. Analysis of jet at 61.475 microseconds

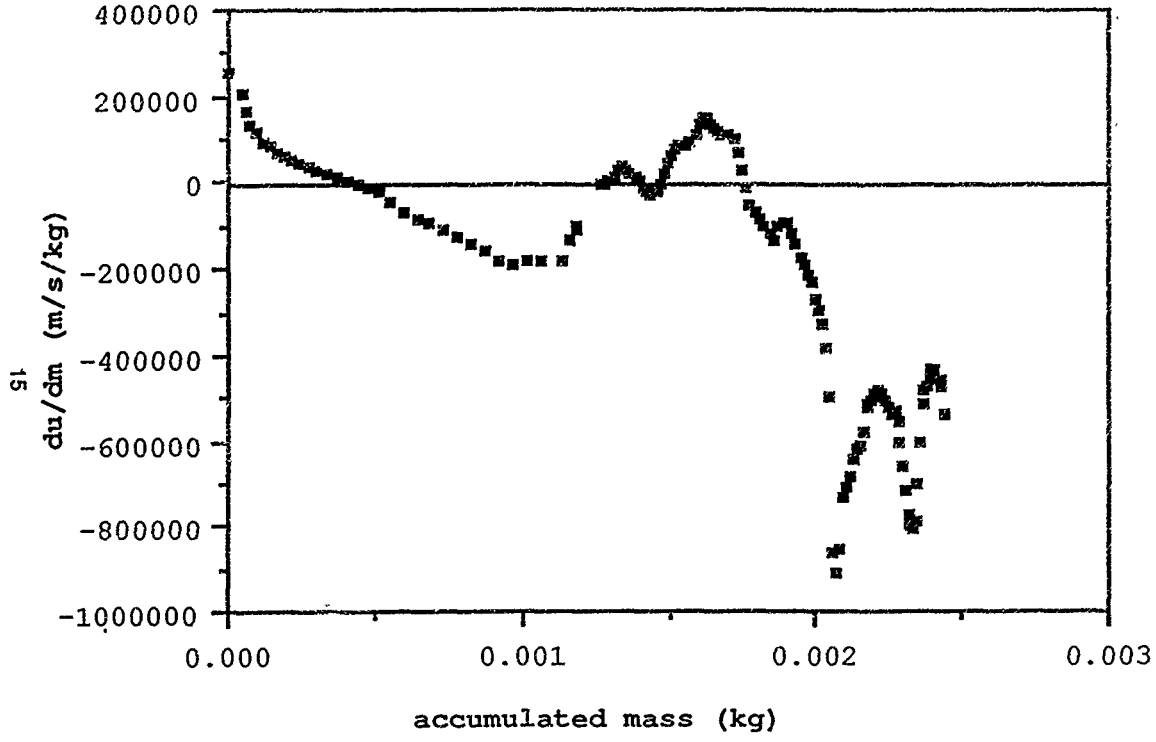

Figure 9. Velocity gradient

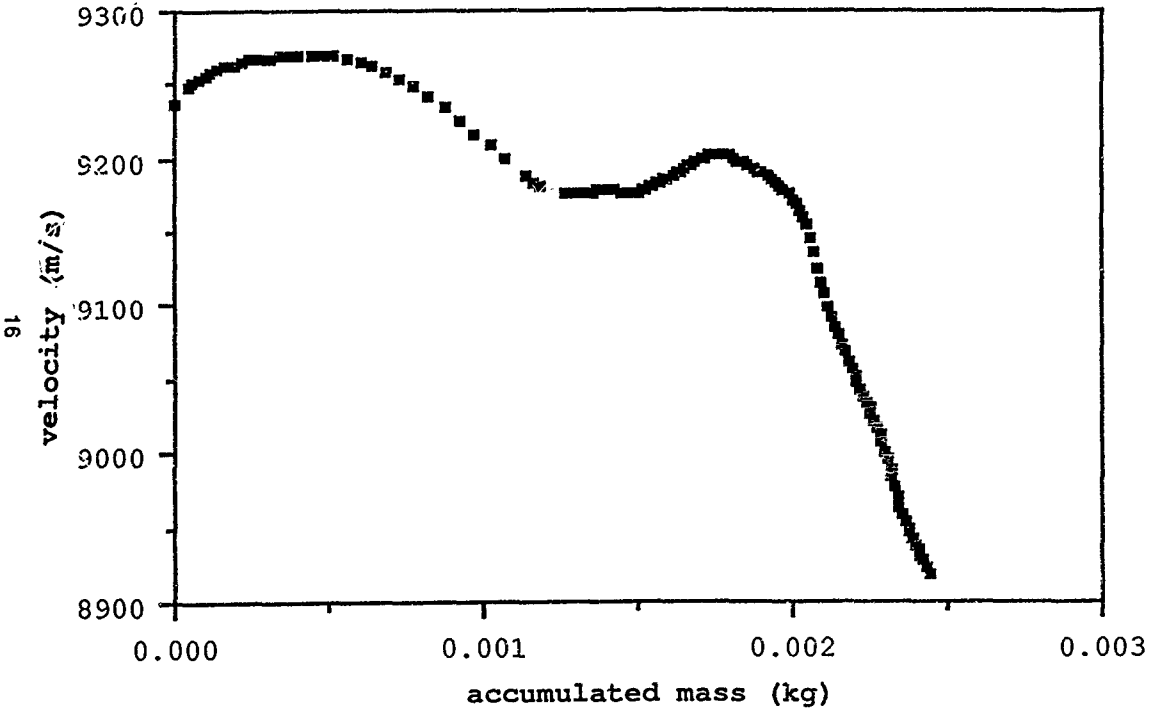

Figure 10. Particle velocity

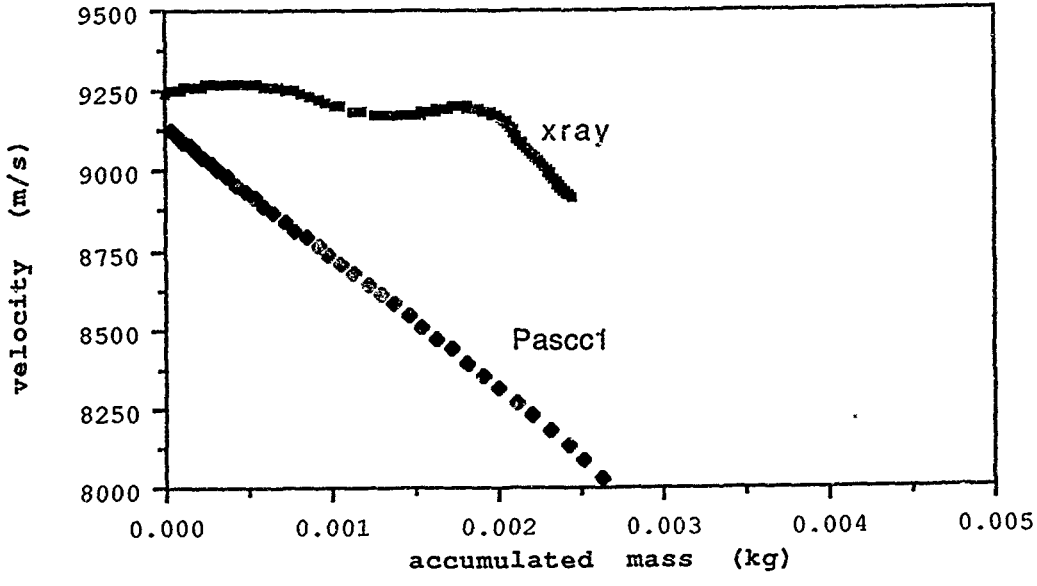

Figure 11. Viper velocity distribution

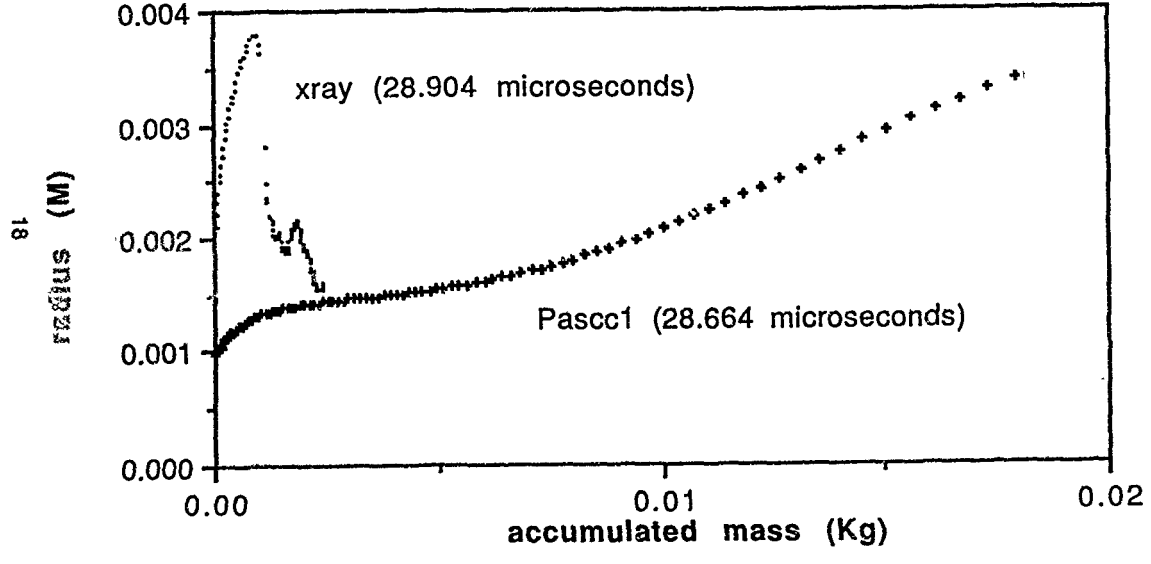

Figure 12. Distribution of jet radius

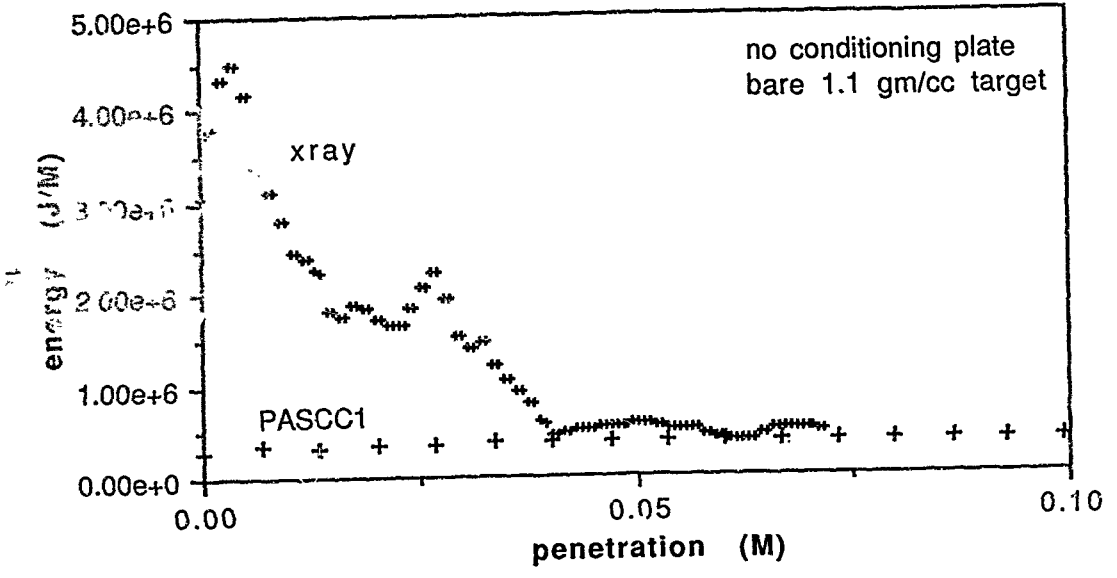

Figure 13. Viper at 14.5 inches

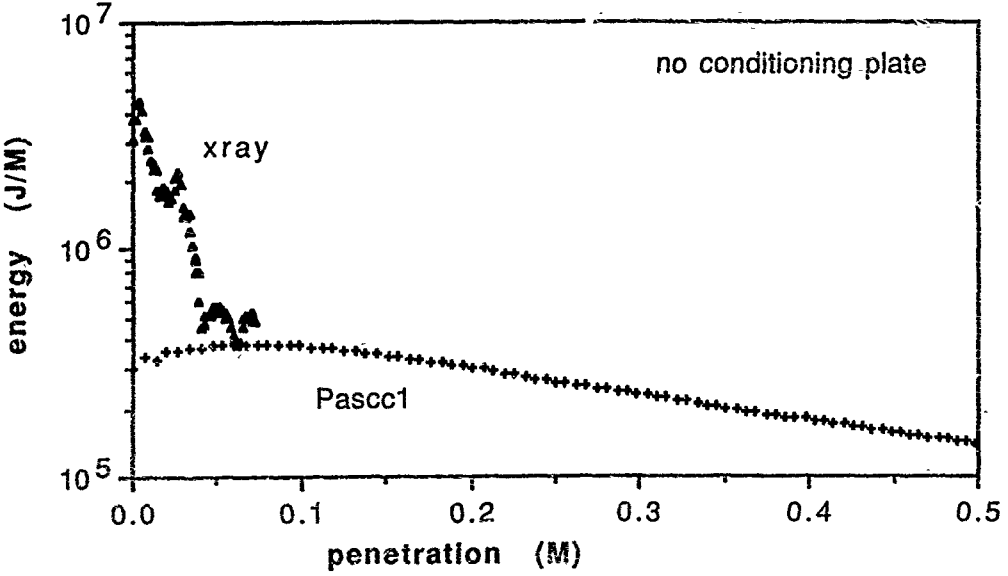

Figure 14. Viper comparisons

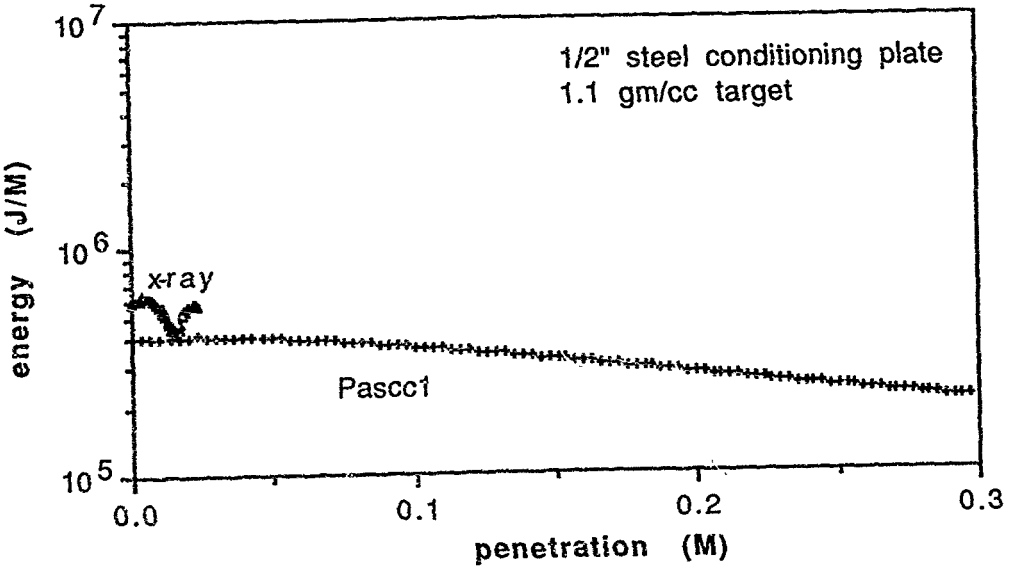

Figure 15. Viper with 1/2 inch plate

REFERENCES

1. Walters, W.P. and Zukas, J.A., Fundamentals of Shaped Charges, John Wiley & Sons, New York, 1989.

2. Baker, Ernest L., A Parametric Optimization of Shaped Charge Wave Shaping, Society for Computer Simulation 1992 Eastern Multi-conference, Military and Government Simulation Conference, 6-9 April 1992.

DISTRIBUTION LIST

Commander
Armament Research, Development and Engineering Center
U.S. Army Armament, Munitions and Chemical Command
ATTN: SMCAR-IMI-I (5)
SMCAR-CO
SMCAR-TD
SMCAR-SF
SMCAR-AEE (3)
SMCAR-AEF-C, R.A. Chevalaz
SMCAR-AEE-WW, B. Fishburn (5)
Picatinny Arsenal, NJ 07806-5000

Administrator
Defense Technical Information Center
ATTN: Accessions Division (12)
Cameron Station
Alexandria, VA 22304-6145

Commander
U.S. Army Armament, Munitions and Chemical Command
ATTN: AMSMC-GCL (D)
Picatinny Arsenal, NJ 07806-5000

Director
U.S. Army Materiel Systems Analysis Activity
ATTN: AMXSY-MP
Aberdeen Proving Ground, MD 21005-5066

Commander
Chemical Research, Development and Engineering Center
U.S. Army Armament, Munitions and Chemical Command
ATTN: SMCCR-MSI
Aberdeen Proving Ground, MD 21010-5423

Commander
Chemical Research, Development and Engineering Center
U.S. Army Armament, Munitions and Chemical Command
ATTN: SMCCR-RSP-A
Aberdeen Proving Ground, MD 21010-5423

Director
Ballistic Research Laboratory
ATTN: AMXBR-OD-ST
SLCBR-TB-EE, E. Frey
G. Gibbons, Jr.
J. Watson
SLCBR-IB-P, A. Barrows
Aberdeen Proving Ground, MD 21005-5066

Chief
Benet Weapons Laboratory, CCAC
Armament Research, Development and Engineering Center
U.S. Army Armament, Munitions and Chemical Command
ATTN: SMCAR-CCB-TL
SMCAR-CCB-DI
Watervliet, NY 12189-5000

Commander
U.S. Army Rock Island Arsenal
ATTN: SMCRI-TL/Technical Library
AMSMC-DS
Rock Island, IL 61299-5000

Director
U.S. Army TRADOC Systems Analysis Activity
ATTN: ATAA-SL
White Sands Missile Range, NM 88002

Director
VLAMO
ATTN: AMSLC-VL-D
Aberdeen Proving Ground, MD 21005-5066